

Multi-set variational quantum dynamics algorithm for simulating nonadiabatic dynamics on quantum computers

Jingjing Li,[†] Weitang Li,[‡] Xiaoxiao Xiao,[†] Limin Liu,[†] Zhendong Li,[†] Jiajun
Ren,^{*,†} and Weihai Fang[†]

[†]*Key Laboratory of Theoretical and Computational Photochemistry, Ministry of Education,
College of Chemistry, Beijing Normal University, Beijing 100875, People's Republic of
China*

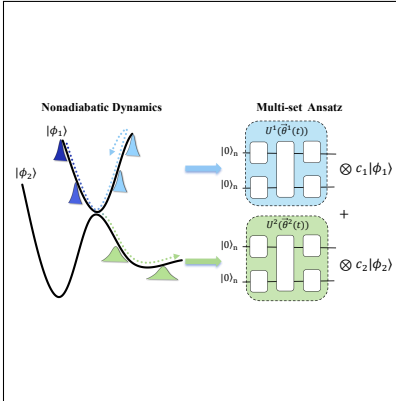
[‡]*School of Science and Engineering, The Chinese University of Hong Kong, Shenzhen,
518172, P. R. China.*

E-mail: jjren@bnu.edu.cn

Abstract

Accelerating quantum dynamical simulations with quantum computing has received considerable attention but remains a significant challenge. In variational quantum algorithms for quantum dynamics, designing an expressive and shallow-depth parameterized quantum circuit (PQC) is a key difficulty. Here, we proposed a multi-set variational quantum dynamics algorithm (MS-VQD) tailored for nonadiabatic dynamics involving multiple electronic states. MS-VQD employs multiple PQCs to represent the electronic-nuclear coupled wavefunction, with each circuit adapting to the motion of nuclear wavepacket on a specific potential energy surface. By simulating excitation energy transfer dynamics in molecular aggregates described by the Frenkel-Holstein model, we demonstrated that MS-VQD achieves the same accuracy as traditional VQD while requiring significantly shallower PQCs. Notably, its advantage increases with the number of electronic states, making it suitable for simulating nonadiabatic quantum dynamics in complex molecular systems.

TOC Graphic



Nonadiabatic dynamics play a crucial role in chemistry, physics, and material science, influencing processes such as photochemical reactions, excitation energy transfer, charge separation, and relaxation.¹⁻⁴ In these processes, quantum effects, including coherence and tunneling, have been identified essential.⁵⁻⁷ However, accurately simulating nonadiabatic dynamics with quantum effects remains a major challenge in theoretical chemistry.^{8,9} In classical computation, exact methods for solving the coupled electronic-nuclear time-dependent Schrödinger equation (TDSE) suffer from exponential growth in complexity and memory with increasing system size, known as the “quantum exponential wall”. Over the past few decades, various approximate but numerically exact methods have been developed to overcome this problem and have made great success.¹⁰⁻¹³ However, their scalability and general applicability remain to be carefully assessed.

The advent of quantum computing offers compelling new avenues to overcome these challenges.¹⁴⁻²⁰ Simulating TDSE is considered one of the most promising applications for demonstrating quantum advantage.²¹ To this end, various quantum algorithms have been proposed,²² including decomposition algorithms and variational algorithms.^{21,23-32} Their applications to different chemical dynamics problems have also emerged, for both closed and open systems.³³⁻⁴⁸ Compared to decomposition algorithms, hybrid quantum-classical variational algorithms require significantly shallower circuit depths and exhibit greater resilience to noise, making them more practical for implementation on near-term quantum hardware. Their feasibility has been validated in recent experimental demonstrations.^{37,41,49}

In variational quantum algorithms,^{50,51} the wavefunction ansatz, implemented as a parameterized quantum circuit (PQC), plays a crucial role in determining both accuracy and efficiency. An effective PQC must satisfy two key criteria: (i) high expressivity, enabling it to represent highly entangled quantum states beyond classical ansatzes, and (ii) short circuit depth, ensuring practical implementation on the current noisy quantum hardware. To meet these requirements, various PQC designs have been proposed,⁵²⁻⁶² including the unitary coupled cluster ansatz for electronic structure problems,⁵² the Hamiltonian variational ansatz,⁵³

hardware-efficient ansatz,⁵⁴ and quantum-classical hybrid ansatz,^{58,62} etc.

Current variational quantum dynamics (VQD) algorithms use a single PQC $U(\vec{\theta}(t))$ to represent the wavefunction of the entire system,^{17,26}

$$|\Psi(t)\rangle_{\text{VQD}} = U(\vec{\theta}(t))|0\rangle. \quad (1)$$

In nonadiabatic dynamics involving multiple electronic states, $U(\vec{\theta}(t))$ entangles both electronic and nuclear degrees of freedom. However, when potential energy surfaces (PESs) have distinct landscapes, the motion of nuclear wavepacket on each PES varies significantly, making it difficult for a single compact PQC to accurately capture the full dynamics. A schematic example is shown in Figure 1(a), where an initial nuclear wavepacket splits into two after passing through a strong nonadiabatic coupling region. On the steeper upper PES, the wavepacket reflects backward, while on the flatter lower PES, it propagates forward. In order to accurately describe the two wavepackets, the PQC should incorporate two distinct ansatz blocks $U^1(\vec{\theta}^1(t))$ and $U^2(\vec{\theta}^2(t))$, controlled by the qubit encoding the electronic state (Figure 1(b)), resulting in a doubled circuit depth.

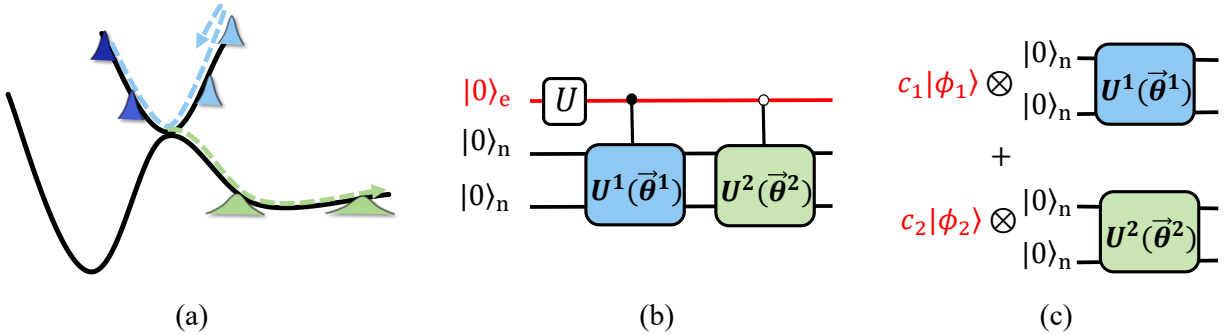


Figure 1: (a) Schematic illustration of a two-state nonadiabatic dynamics process. One wavepacket splits into two upon passing through a strong nonadiabatic coupling region. (b) In variational quantum dynamics, two distinct ansatz blocks are employed, determined by the electronic state index, resulting in a doubled circuit depth. (c) In multi-set variational quantum dynamics, two separate circuits are used, each representing the nuclear wavepacket on a specific potential energy surface.

To address this challenge, in this study, we proposed a multi-set variational quantum

dynamics algorithm (MS-VQD), an extension of the original VQD framework tailored for multi-state dynamics, inspired by the classical multi-set tensor network ansatz.⁶³ We demonstrated the effectiveness of MS-VQD in simulating excitation energy transfer (EET) dynamics in molecular aggregates described by the Frenkel-Holstein model. EET plays a fundamental role in light-harvesting complexes and organic solar cells.^{3,5} Our results showed that MS-VQD achieves the same accuracy as conventional VQD while requiring significantly shallower PQCs. Notably, its advantage becomes more pronounced as the number of electronic states increases, making it particularly well-suited for complex nonadiabatic quantum dynamics simulations.

The wavefunction ansatz of MS-VQD is

$$|\Psi(t)\rangle_{\text{MS-VQD}} = \sum_p c_p(t) |\phi_p\rangle_{\text{e}} |\chi_p(t)\rangle_{\text{n}}, \quad (2)$$

$$|\chi_p(t)\rangle_{\text{n}} = U^p(\vec{\theta}^p(t)) |\mathbf{0}\rangle_{\text{n}}, \quad (3)$$

where the subscript e/n indicates electronic/nuclear wavefunction. MS-VQD employs separate PQCs, $U^p(\vec{\theta}^p(t))$, each independently representing the nuclear wavepacket $|\chi_p\rangle$ associated with the p th electronic state $|\phi_p\rangle$. These wavepackets are then multiplied by their respective electronic states and linearly combined to reconstruct the full wavefunction (Figure 1(c)). This structure allows each PQC to better adapt to its corresponding wavepacket, resulting in a more compact and efficient ansatz.

The nonadiabatic Hamiltonian in the diabatic representation can be generally expressed as

$$\hat{H} = \hat{T} + \begin{bmatrix} \hat{V}_{11} & \hat{V}_{12} & \cdots & \hat{V}_{1N} \\ \hat{V}_{21} & \hat{V}_{22} & \cdots & \hat{V}_{2N} \\ \cdots & \cdots & \cdots & \cdots \\ \hat{V}_{N1} & \hat{V}_{N2} & \cdots & \hat{V}_{NN} \end{bmatrix}. \quad (4)$$

The diabatic energies and coupling terms depend on the nuclear coordinates $\hat{V}_{pq} \equiv \hat{V}_{pq}(\vec{R})$.

Based on the McLachlan's time-dependent variational principle $\delta||(\hat{H} - i\partial/\partial t)|\Psi(\vec{\theta}(t))||^2 = 0$,⁶⁴ the equations of motion of MS-VQD is

$$\sum_k |c_p|^2 \text{Re}(A_{lk}^{pp} - D_l^{pp} D_k^{pp*}) \dot{\theta}_k^p = \text{Im} \sum_q c_p^* c_q (B_l^{pq} - H_{pq} D_l^{pp}) \quad (5)$$

$$\dot{c}_p + c_p \sum_k D_k^{pp*} \dot{\theta}_k^p + i \sum_q c_q H_{pq} = 0, \quad (6)$$

where the matrices $\mathbf{A}, \mathbf{B}, \mathbf{D}, \mathbf{H}$ are:

$$A_{lk}^{pp} = \left\langle \frac{\partial \chi_p}{\partial \theta_l^p} \middle| \frac{\partial \chi_p}{\partial \theta_k^p} \right\rangle \quad (7)$$

$$B_l^{pq} = \left\langle \frac{\partial \chi_p}{\partial \theta_l^p} \middle| \hat{T} + \hat{V}_{pq} \middle| \chi_q \right\rangle \quad (8)$$

$$D_k^{pp} = \left\langle \frac{\partial \chi_p}{\partial \theta_k^p} \middle| \chi_p \right\rangle \quad (9)$$

$$H_{pq} = \langle \chi_p | \hat{T} + \hat{V}_{pq} | \chi_q \rangle. \quad (10)$$

The detailed derivation is provided in the Appendix. The matrix elements of $\mathbf{A}, \mathbf{B}, \mathbf{D}, \mathbf{H}$ can be measured using either the direct measurement or the Hadamard test algorithm, as illustrated in Figure 2(a). The details are presented in Section 1 and Figure S1 of Supporting Information (SI). When only a single electronic state is present, eqs (5) and (6) reduce to a simplified form,

$$\sum_k \text{Re}(A_{lk} - D_l D_k^*) \dot{\theta}_k = \text{Im}(B_l - E D_l), \quad (11)$$

$$\dot{c} + c \sum_k D_k \dot{\theta}_k + i c E = 0. \quad (12)$$

Eq (11) is consistent with the equation of motion for traditional VQD, as derived in the previous studies.²⁶ At first glance, MS-VQD appears more complex than VQD due to the additional index p , which corresponds to a specific electronic state. However, the left-hand

side of the linear equation eq (5) depends only on p , resulting in a block-diagonal structure. This simplifies solving the linear equation on a classical computer. The overall processes of MS-VQD is illustrated in Figure 2(a), including:

- (i) Initialize \vec{c} and $\vec{\theta}$ according to the initial condition;
- (ii) Prepare PQC on quantum computer and measure the matrix elements of $\mathbf{A}, \mathbf{B}, \mathbf{D}, \mathbf{H}$;
- (iii) Calculate the time derivative $\dot{\vec{\theta}}$ and $\dot{\vec{c}}$ according to eqs (5) (6) and update $\vec{\theta}$ and \vec{c} with any proper solver for initial value problems on classical computer. Return back to (ii).

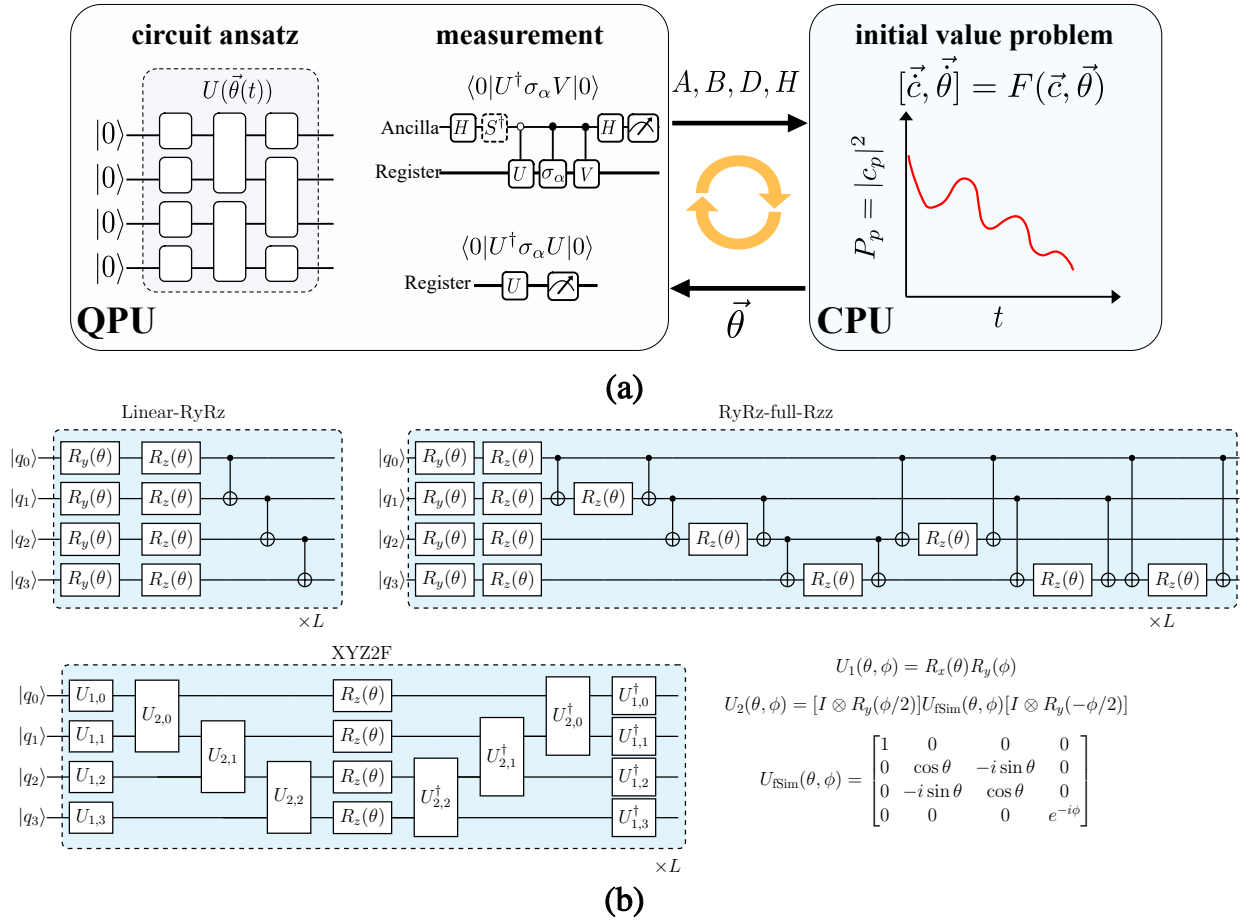


Figure 2: (a) Workflow of the hybrid quantum-classical multi-set variational quantum dynamics algorithm. The quantum computer prepares the nuclear wavepacket and measures the matrix elements using direct measurement or the Hadamard test algorithm. The classical computer updates the parameters by solving an initial value problem. (b) Three types of ansatzes used in this study: linear-RyRz ansatz, RyRz-full-Rzz ansatz, and XYZ2F ansatz.

To evaluate the effectiveness of MS-VQD in simulating nonadiabatic quantum dynamics, we applied it to model the excitation energy transfer dynamics in one-dimensional molecular aggregates using the Frenkel-Holstein model Hamiltonian, which is

$$\begin{aligned}\hat{H} = & \sum_p \varepsilon_p |\phi_p\rangle \langle \phi_p| + \sum_p J(|\phi_p\rangle \langle \phi_{p+1}| + |\phi_{p+1}\rangle \langle \phi_p|) \\ & + \sum_{pm} \omega_m \hat{b}_{pm}^\dagger \hat{b}_{pm} + \sum_{pm} g_m \omega_m |\phi_p\rangle \langle \phi_p| (\hat{b}_{pm}^\dagger + \hat{b}_{pm}).\end{aligned}\quad (13)$$

In this model, ε_p denotes the excitation energy of the local electronic state $|\phi_p\rangle$, J denotes the excitonic coupling. \hat{b}_{pm}^\dagger and \hat{b}_{pm} correspond to the creation and annihilation operators of the m th vibrational mode of the p th molecule, with frequency ω_m and dimensionless electron-vibration coupling constant g_m .

To encode the infinitely large bosonic Hilbert space into qubits, we truncated the local bosonic energy levels to a finite size d and mapped them to qubit states using Gray code. For example, when $d = 4$, the encoding follows $|00\rangle \rightarrow |0\rangle$, $|01\rangle \rightarrow |1\rangle$, $|11\rangle \rightarrow |2\rangle$, and $|10\rangle \rightarrow |3\rangle$. Gray code has been shown to not only reduce the number of qubits compared to unary encoding but also reduce the number of two-qubit gates needed to represent b^\dagger/b compared to standard binary encoding.⁶⁵ In addition, MS-VQD is also compatible with the recently proposed variational encoding method, which can further reduce qubit requirements.⁶⁶ Besides encoding the bosonic state, in traditional VQD, electronic states are encoded using binary code. For a system with N molecules and K nuclear degrees of freedom per molecule, since MS-VQD does not explicitly encode electronic states on the quantum computer, the number of qubits is reduced from $NK \log_2 d + \log_2 N$ in VQD to $NK \log_2 d$. Meanwhile, the number of Hamiltonian terms after mapping into qubits in MS-VQD is also much less than that in VQD shown in Figure S2.

In the choice of ansatz for each PQC in both VQD and MS-VQD, any proper ansatz can be used. We employed three types: the linear-RyRz ansatz,⁵⁷ the RyRz-full-Rzz ansatz, and the XYZ2F ansatz,⁶¹ as shown in Figure 2(b). The first two are simple hardware

efficient ansatzes, where single-qubit rotation gates and two-qubit CNOT/Rzz gates are placed in alternation. The third, XYZ2F, is a recently developed ansatz⁶¹ that satisfies key physical constraints and has been proven to be universal, systematically improvable, and size-consistent. In our calculations, the number of layers L of these ansatzes are gradually increased to enhance the expressivity.

We primarily focused on the exciton population dynamics, defined as $P_p(t) = |\langle \phi_p | \Psi(t) \rangle|^2$. The initial condition assumes that the exciton is localized on the first molecule, with all vibrational modes in their ground state. In MS-VQD, $P_p = |c_p|^2$, which can be directly computed classically, whereas in VQD, P_p is obtained by sampling the qubits encoding the electronic state, expressed as $P(j_1 j_2 \cdots, p = \sum_k j_k 2^k)$. All simulations were performed without noise using the quantum simulator TensorCircuit⁶⁷ and TenCirChem.⁶⁸ Reference data was calculated using the numerically exact time-dependent density matrix renormalization group algorithm (TD-DMRG).¹³

Figure 3 presents the exciton population P_1 of the first molecule for dimer ($N = 2$) and hexamer ($N = 6$), using the linear-RyRz ansatz with $L = 1, 2, 3$ layers. One vibrational mode per molecule is considered. The parameters used are $g = 1$, $J = -1$, $d = 2$, $dt = 0.1$, with $\omega = 1$ as the unit. Comparing Figure 3(a) to (c) and (b) to (d), we observed that as the number of molecules increases, the simulation becomes more challenging, requiring additional ansatz layers to maintain accuracy for both VQD and MS-VQD. Compared to VQD, MS-VQD consistently achieves higher accuracy with the same L , regardless of system size. Similar behaviors were observed for the other two ansatzes, as shown in Figure S3 and S4.

To quantitatively assess the performance of MS-VQD and VQD across different system sizes, we defined the population error as

$$\varepsilon = \frac{\sum_{k=1}^{N_{\text{steps}}} |P_1(t_k) - P_1^{\text{ref}}(t_k)|}{N_{\text{steps}}}. \quad t \in [0, 10/\omega] \quad (14)$$

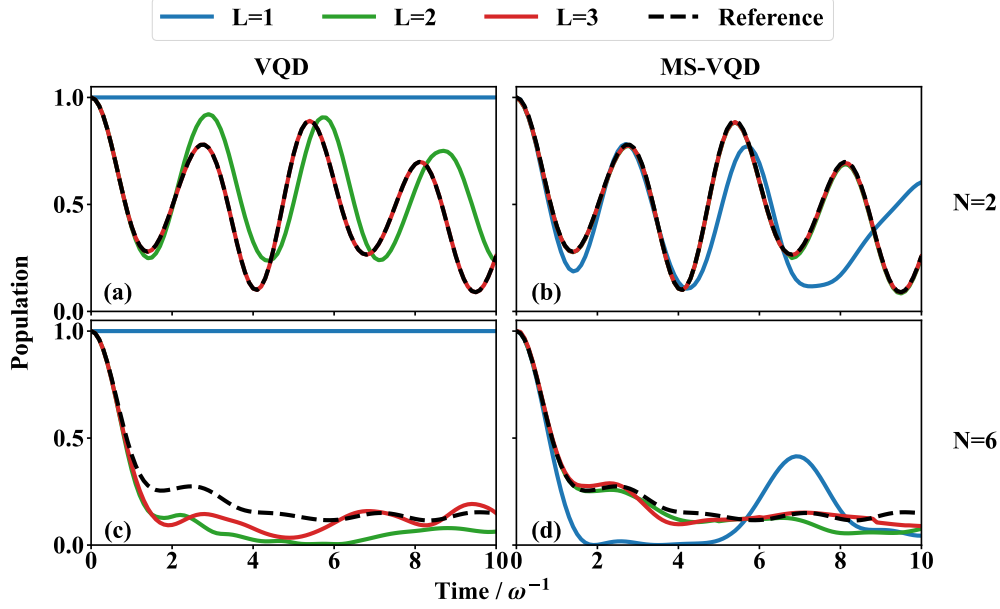


Figure 3: The exciton population on the first molecule as a function of time, $|\langle\phi_1|\Psi(t)\rangle|^2$. (a) and (b) Results of VQD (a) and MS-VQD (b) for the dimer model. Different colors represent different layers of the ansatz, with $L = 1, 2, 3$. The dashed black curve shows the reference results calculated by the time-dependent density matrix renormalization group algorithm. (c) and (d) Similar to (a) and (b), but for the hexamer model. The linear-RyRz ansatz is used.

Figure 4(a-c) illustrate how the error evolves with an increasing number of ansatz layers L for the three different ansatzes (The error at $L = 0$ is arbitrarily set to 1 for eye guidance). Regardless of the ansatz used, MS-VQD exhibits faster convergence with L compared to VQD. For example, in the case of an octamer using the linear-RyRz ansatz, MS-VQD with $L = 4$ achieves higher accuracy than VQD with $L = 16$. Similar trends are observed for both the RyRz-full-Rzz and XYZ2F ansatzes, suggesting that the advantage of MS-VQD is likely generalizable across other ansatz choices. When comparing the three ansatzes within MS-VQD, the RyRz-full-Rzz ansatz performs slightly better than the linear-RyRz ansatz in terms of PQC layers. For the octamer with $L = 16$, the error of the RyRz-full-Rzz ansatz is 5.0×10^{-4} , while that of the linear-RyRz ansatz is 2.0×10^{-3} . The XYZ2F ansatz performs much better, achieving an error of 3.8×10^{-4} with only $L = 8$. This trend is consistent with the findings from ground-state calculations.⁶¹ We also used the wavefunction infidelity $1 - \text{Re}\langle\Psi^{\text{ref}}(t)|\Psi(t)\rangle$ as the error metric, the findings are similar as shown in Figure S5.

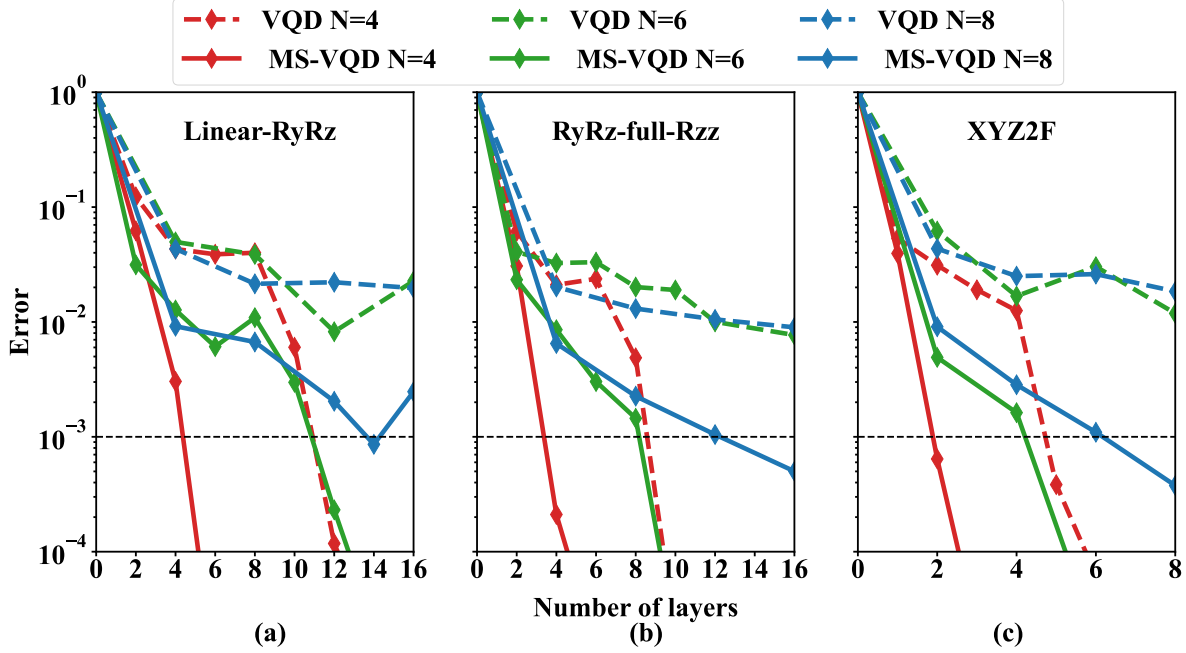


Figure 4: The population error for different layers of ansatz in VQD and MS-VQD. (a) Linear-RyRz ansatz, (b) RyRz-full-Rzz ansatz, and (c) XYZ2F ansatz. Different colors represent different system sizes.

Figure 5 summarizes the number of layers L required to achieve a population error below 10^{-3} for different system sizes. As system size increases, VQD struggles to maintain accuracy, requiring a rapidly growing number of layers. In contrast, MS-VQD scales much more favorably, requiring far fewer layers to achieve the same accuracy. This trend is consistent across all three ansatzes, further highlighting the superiority of MS-VQD for nonadiabatic dynamics involving a large number of electronic states. Regarding the number of parameters in the ansatzes, MS-VQD requires slightly fewer parameters than VQD (shown in Figure S6), meaning its PQC depth is approximately $1/N$ of that in VQD to achieve the same accuracy. This finding aligns with the schematic diagram in Figure 1, illustrating that VQD requires N ansatz blocks to capture the dynamics of N electronic states accurately. However, the number of parameters only becomes smaller than the size of the full Hilbert space when the system is larger than hexamer (Figure S7), indicating that quantum advantage may only emerge for studying large systems.

Due to the exponentially large computational cost of classical simulations of quantum

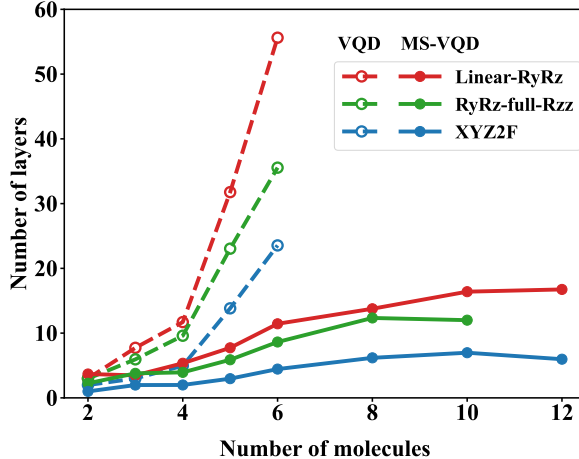


Figure 5: The required number of ansatz layers L for different system sizes to achieve an error below 10^{-3} . Solid lines represent MS-VQD results, while dashed lines represent VQD. Different colors denote different ansatzes.

computing, the above calculations for large molecular aggregates are restricted to local bosonic levels $d = 2$. However, this truncation is not sufficient for accurately representing real molecular aggregates. Therefore, we evaluated the performance of VQD and MS-VQD with different d on a molecular dimer. After mapping the Hamiltonian to qubits, the total number of terms increases linearly with d (Figure S1(a)), indicating that a larger d will result in a more entangled state and thus deeper PQC. Since MS-VQD involves fewer Hamiltonian terms than VQD, it is expected that MS-VQD requires a shallower PQC. As shown in Figure 6, as d increases, the number of ansatz layers required for MS-VQD to achieve an error below 10^{-3} grows much more slowly compared to VQD. This suggests that MS-VQD maintains its computational advantage even with large local bosonic space.

Furthermore, we examined the robustness of MS-VQD across different coupling regimes and varying numbers of vibrational modes, as detailed in SI Section 6. Figure S8 and S9 demonstrated that the advantage of MS-VQD over VQD remains robust across different electronic and electron-vibration coupling strengths, as well as for multiple numbers of vibrational modes.

Finally, we analyzed the computational cost of VQD and MS-VQD. The scaling of circuit depth and the number of measurements with respect to the number of ansatz layers L

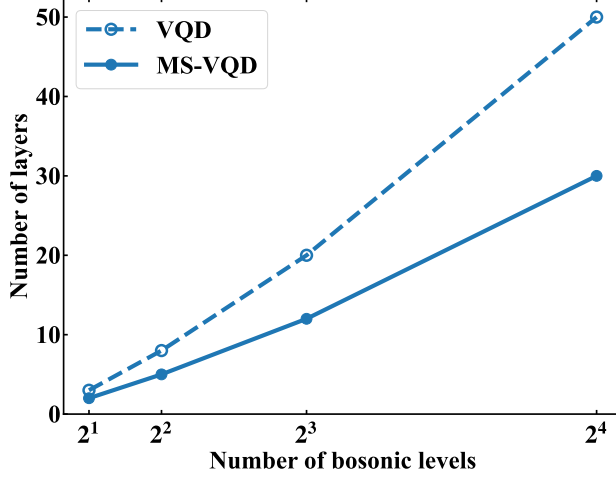


Figure 6: The required number of ansatz layers to achieve an error below 10^{-3} for different numbers of local bosonic levels d .

Table 1: The circuit depth and the number of measurements required to calculate the matrices A , D , B , and H .

Algorithm		A_{lk}^{pp}	D_k^{pp}	B_l^{pq}	H_{pq}
VQD	depth	$\mathcal{O}(L)$	$\mathcal{O}(L)$	$\mathcal{O}(L)$	$\mathcal{O}(L)$
	times	$\mathcal{O}(n_\theta^2)$	$\mathcal{O}(n_\theta)$	$\mathcal{O}(fn_\theta)$	$\mathcal{O}(f)$
MS-VQD	depth	$\mathcal{O}(L/N)$	$\mathcal{O}(L/N)$	$\mathcal{O}(\beta L/N)$	$\mathcal{O}(\beta L/N)$
	times	$\mathcal{O}(n_\theta^2/N)$	$\mathcal{O}(n_\theta)$	$\mathcal{O}(fn_\theta/N)$	$\mathcal{O}(f)$

and the number of parameters n_θ is summarized in Table 1. N is the number of electronic states. For VQD, using either direct measurement or the Hadamard test algorithm, the circuit depth required to compute A_{lk} , D_k , B_l , and E is $\mathcal{O}(L)$. The corresponding number of measurements required is $\mathcal{O}(n_\theta^2)$, $\mathcal{O}(n_\theta)$, $\mathcal{O}(fn_\theta)$, and $\mathcal{O}(f)$, respectively, where f is the number of Hamiltonian terms after mapping to qubits. In comparison, assuming that the number of parameters in MS-VQD is the same as that in VQD to achieve the same accuracy, the ansatz layers required for MS-VQD is $1/N$ of that for VQD. Hence, the circuit depth required to measure the electronic diagonal elements A_{lk}^{pp} and D_k^p in MS-VQD is both $\mathcal{O}(L/N)$. However, for the electronic non-diagonal elements B_l^{pq} and H_{pq} , all gates with parameters must be controlled by an ancilla qubit in the Hadamard test, introducing an overhead prefactor β . For example, a controlled-Ry gate can be decomposed into two Ry

gates plus two CNOT gates, giving $\beta = 4$. This results in a circuit depth of $\mathcal{O}(\beta L/N)$. The number of measurements required to obtain A_{lk}^{pp} and D_k^p is $\mathcal{O}((n_\theta/N)^2 \times N) = \mathcal{O}(n_\theta^2/N)$ and $\mathcal{O}(n_\theta/N \times N) = \mathcal{O}(n_\theta)$, respectively. The number of measurements required for H_{pq} seems to be $\mathcal{O}(fN^2)$, but since only the subset $\hat{T} + \hat{V}_{pq}$ of the whole Hamiltonian \hat{H} needs to be measured for each pq pair, the overall cost remains $\mathcal{O}(f)$. A similar argument applies to B_l^{pq} , which requires $\mathcal{O}(fn_\theta/N)$ measurements. Thus, while the equation of motion for MS-VQD seems more complex than that of VQD, both the circuit depth and the number of measurements of some matrix elements benefit from a $1/N$ reduction. This advantage becomes particularly useful as the number of electronic states increases.

In this letter, we proposed a novel multi-set variational quantum dynamics algorithm for simulating nonadiabatic quantum dynamics and derived the equations of motion within the framework of McLachlan’s time-dependent variational principle for the first time. This is the main contribution of our work. The MS-VQD algorithm utilizes a set of parameterized quantum circuits to represent the entire electronic-nuclear coupled wavefunction, where each PQC corresponds to the wavepacket on a single potential energy surface. This structure allows the ansatz to better adapt to the landscape of different PESs, making the PQCs more compact. Through simulations of the Frenkel-Holstein electron-vibration coupling model, we found that the ansatz depth required by MS-VQD is approximately reduced to $1/N$ of that in VQD while maintaining the same accuracy. This reduction in quantum resource requirements makes MS-VQD more suitable for implementation on current noisy quantum computers. Moreover, the advantage of MS-VQD over VQD is robust across different ansatz choices, sizes of the local bosonic space, coupling regimes, and number of vibrational modes. In the future, MS-VQD can also be extended to imaginary-time evolution⁶⁹ for calculating quantum statistical properties. Additionally, it can be combined with grid basis to study nonadiabatic dynamics on real anharmonic potential energy surfaces.^{33,70} Despite its advantages, some challenges remain. Although MS-VQD outperforms VQD in simulating nonadiabatic dynamics, achieving highly accurate results still requires a large number of

parameters. For large molecular aggregates that may exhibit quantum advantage, the quantum resources required by all three hardware-efficient ansatzes explored in this study have exceeded the capabilities of current noisy quantum computers. Given MS-VQD’s strength in adapting to wavepackets on each PES, exploring independent and adaptive ansatz^{56,71,72} for each PQC to replace the shared and fixed ansatz may further compact the circuit and enhance efficiency.

Appendix: Derivation of MS-VQD

Let any vector on the tangent space of $|\Psi(\vec{\theta}(t))\rangle$ be denoted as φ . According to McLachlan’s time-dependent variational principle, the optimal solution for $\dot{\Psi}(\vec{\theta}(t))$ is the vector φ that minimizes the functional \mathcal{F} ,

$$\mathcal{F} = \|\varphi + i\hat{H}\Psi(\vec{\theta}(t))\|^2 \quad (15)$$

The minimal point satisfies

$$\delta\mathcal{F} = \langle \delta\varphi | \dot{\Psi}(\vec{\theta}(t)) + i\hat{H}\Psi(\vec{\theta}(t)) \rangle + \text{h.c.} = 0 \quad (16)$$

For the multi-set wavefunction ansatz,

$$\dot{\Psi}(\vec{\theta}(t)) = \sum_q \dot{c}_q \phi_q \chi_q + \sum_{qk} c_q \phi_q \frac{\partial \chi_q}{\partial \theta_k^q} \dot{\theta}_k^q \quad (17)$$

$$\delta\varphi = \sum_p \delta a_p \phi_p \chi_p + \sum_{pl} c_p \phi_p \frac{\partial \chi_p}{\partial \theta_l^p} \delta b_l^p \quad (18)$$

Note that while δa_p can be complex, δb_l^p must be real, as required by the quantum computer. Substituting eq (17) and (18) into eq (16), we obtain

$$\left\langle \sum_p \delta a_p \phi_p \chi_p + \sum_{pl} c_p \phi_p \frac{\partial \chi_p}{\partial \theta_l^p} \delta b_l^p \left| \sum_q \dot{c}_q \phi_q \chi_q + \sum_{qk} c_q \phi_q \frac{\partial \chi_q}{\partial \theta_k^q} \dot{\theta}_k^q + i \hat{H} \sum_q c_q \phi_q \chi_q \right. \right\rangle + \text{h.c.} = 0 \quad (19)$$

The above formula can be separated into three parts: δa_p , δa_p^* (since δa_p is complex, δa_p and δa_p^* can be treated as independent variations), and δb_l^p . Using the relation $\langle \phi_p | \phi_q \rangle = \delta_{pq}$, these three parts are given by:

1. δa_p part:

$$\dot{c}_p + c_p \sum_k D_k^{pp*} \dot{\theta}_k^p + i \sum_q c_q H_{pq} = 0 \quad (20)$$

2. δa_p^* part:

$$\dot{c}_p^* + c_p^* \sum_k D_k^{pp} \dot{\theta}_k^p - i \sum_q c_q^* H_{pq}^* = 0 \quad (21)$$

Comparing eq (20) and eq (21), we see that if one expression holds, the other must also be valid. Therefore, it is sufficient to consider only one of them.

3. δb_l^p part:

$$c_p^* \left\langle \frac{\partial \chi_p}{\partial \theta_l^p} \left| \dot{c}_p \chi_p \right. \right\rangle + c_p^* \left\langle \frac{\partial \chi_p}{\partial \theta_l^p} \left| \sum_k c_p \frac{\partial \chi_p}{\partial \theta_k^p} \dot{\theta}_k^p \right. \right\rangle + c_p^* \left\langle \frac{\partial \chi_p}{\partial \theta_l^p} \left| i \sum_q (\hat{T} + \hat{V}_{pq}) c_q \chi_q \right. \right\rangle + \text{h.c.} = 0 \quad (22)$$

Substituting \dot{c}_p from eq (20) into eq (22), we obtain eq (5) in the main text.

Acknowledgement

This work is supported by the Innovation Program for Quantum Science and Technology (Grant No. 2023ZD0300200), NSAF (Grant No. U2330201), the National Natural Science Foundation of China (Grant No. 22273005), and the Fundamental Research Funds for the Central Universities.

Supporting Information Available

The circuits to measure matrix elements in MS-VQD; The number of Hamiltonian terms after mapping to qubits; The population dynamics with RyRz-full-Rzz ansatz and XYZ2F ansatz; Infidelity as a function of the number of ansatz layers; The number of parameters in MS-VQD and VQD; The performance of MS-VQD and VQD with different coupling strength and number of modes.

References

- (1) Yarkony, D. R. Nonadiabatic Quantum Chemistry- Past, Present, and Future. *Chemical reviews* **2012**, *112*, 481–498.
- (2) Long, R.; Prezhdo, O. V.; Fang, W. Nonadiabatic charge dynamics in novel solar cell materials. *Wiley Interdisciplinary Reviews: Computational Molecular Science* **2017**, *7*, e1305.
- (3) Jang, S. J.; Mennucci, B. Delocalized excitons in natural light-harvesting complexes. *Reviews of Modern Physics* **2018**, *90*, 035003.
- (4) Dimitriev, O. P. Dynamics of excitons in conjugated molecules and organic semiconductor systems. *Chemical Reviews* **2022**, *122*, 8487–8593.

- (5) Brédas, J.-L.; Sargent, E. H.; Scholes, G. D. Photovoltaic concepts inspired by coherence effects in photosynthetic systems. *Nature materials* **2017**, *16*, 35–44.
- (6) Wang, L.; Allodi, M. A.; Engel, G. S. Quantum coherences reveal excited-state dynamics in biophysical systems. *Nature Reviews Chemistry* **2019**, *3*, 477–490.
- (7) Schultz, J. D.; Yuly, J. L.; Arsenault, E. A.; Parker, K.; Chowdhury, S. N.; Dani, R.; Kundu, S.; Nuomin, H.; Zhang, Z.; Valdiviezo, J. et al. Coherence in Chemistry: Foundations and Frontiers. *Chemical reviews* **2024**, *124*, 11641–11766.
- (8) Tully, J. C. Perspective: Nonadiabatic dynamics theory. *The Journal of chemical physics* **2012**, *137*.
- (9) Curchod, B. F.; Martínez, T. J. Ab initio nonadiabatic quantum molecular dynamics. *Chemical reviews* **2018**, *118*, 3305–3336.
- (10) Makri, N. Quantum dissipative dynamics: A numerically exact methodology. *The Journal of Physical Chemistry A* **1998**, *102*, 4414–4427.
- (11) Worth, G. A.; Meyer, H.-D.; Köppel, H.; Cederbaum, L.; Burghardt, I. Using the MCTDH wavepacket propagation method to describe multimode non-adiabatic dynamics. *International Reviews in Physical Chemistry* **2008**, *27*, 569–606.
- (12) Tanimura, Y. Numerically “exact” approach to open quantum dynamics: The hierarchical equations of motion (HEOM). *The Journal of chemical physics* **2020**, *153*.
- (13) Ren, J.; Li, W.; Jiang, T.; Wang, Y.; Shuai, Z. Time-dependent density matrix renormalization group method for quantum dynamics in complex systems. *Wiley Interdisciplinary Reviews: Computational Molecular Science* **2022**, *12*, e1614.
- (14) Cao, Y.; Romero, J.; Olson, J. P.; Degroote, M.; Johnson, P. D.; Kieferová, M.; Kivlichan, I. D.; Menke, T.; Peropadre, B.; Sawaya, N. P. et al. Quantum chemistry in the age of quantum computing. *Chemical reviews* **2019**, *119*, 10856–10915.

- (15) Bauer, B.; Bravyi, S.; Motta, M.; Chan, G. K.-L. Quantum algorithms for quantum chemistry and quantum materials science. *Chemical reviews* **2020**, *120*, 12685–12717.
- (16) McArdle, S.; Endo, S.; Aspuru-Guzik, A.; Benjamin, S. C.; Yuan, X. Quantum computational chemistry. *Reviews of Modern Physics* **2020**, *92*, 015003.
- (17) Ollitrault, P. J.; Miessen, A.; Tavernelli, I. Molecular quantum dynamics: A quantum computing perspective. *Accounts of Chemical Research* **2021**, *54*, 4229–4238.
- (18) Motta, M.; Rice, J. E. Emerging quantum computing algorithms for quantum chemistry. *Wiley Interdisciplinary Reviews: Computational Molecular Science* **2022**, *12*, e1580.
- (19) Delgado-Granados, L. H.; Krogmeier, T. J.; Sager-Smith, L. M.; Avdic, I.; Hu, Z.; Sajjan, M.; Abbasi, M.; Smart, S. E.; Narang, P.; Kais, S. et al. Quantum Algorithms and Applications for Open Quantum Systems. *Chemical Reviews* **2025**, *125*, 1823–1839.
- (20) Fauseweh, B. Quantum many-body simulations on digital quantum computers: State-of-the-art and future challenges. *Nature Communications* **2024**, *15*, 2123.
- (21) Lloyd, S. Universal quantum simulators. *Science* **1996**, *273*, 1073–1078.
- (22) Miessen, A.; Ollitrault, P. J.; Tacchino, F.; Tavernelli, I. Quantum algorithms for quantum dynamics. *Nature Computational Science* **2023**, *3*, 25–37.
- (23) Childs, A. M.; Wiebe, N. Hamiltonian simulation using linear combinations of unitary operations. *Quantum Inf. Comput.* **2012**, *12*, 901–924.
- (24) Berry, D. W.; Childs, A. M.; Cleve, R.; Kothari, R.; Somma, R. D. Simulating Hamiltonian dynamics with a truncated Taylor series. *Physical review letters* **2015**, *114*, 090502.
- (25) Li, Y.; Benjamin, S. C. Efficient variational quantum simulator incorporating active error minimization. *Physical Review X* **2017**, *7*, 021050.

- (26) Yuan, X.; Endo, S.; Zhao, Q.; Li, Y.; Benjamin, S. C. Theory of variational quantum simulation. *Quantum* **2019**, *3*, 191.
- (27) Campbell, E. Random compiler for fast Hamiltonian simulation. *Physical review letters* **2019**, *123*, 070503.
- (28) Cirstoiu, C.; Holmes, Z.; Iosue, J.; Cincio, L.; Coles, P. J.; Sornborger, A. Variational fast forwarding for quantum simulation beyond the coherence time. *npj Quantum Information* **2020**, *6*, 82.
- (29) Hu, Z.; Xia, R.; Kais, S. A quantum algorithm for evolving open quantum dynamics on quantum computing devices. *Scientific reports* **2020**, *10*, 3301.
- (30) Barison, S.; Vicentini, F.; Carleo, G. An efficient quantum algorithm for the time evolution of parameterized circuits. *Quantum* **2021**, *5*, 512.
- (31) Schlimgen, A. W.; Head-Marsden, K.; Sager, L. M.; Narang, P.; Mazziotti, D. A. Quantum simulation of the Lindblad equation using a unitary decomposition of operators. *Physical Review Research* **2022**, *4*, 023216.
- (32) Wan, L.; Liu, J.; Li, Z.; Yang, J. Hybrid Hamiltonian Simulation for Excitation Dynamics. *The Journal of Physical Chemistry Letters* **2024**, *15*, 11234–11243.
- (33) Kassal, I.; Jordan, S. P.; Love, P. J.; Mohseni, M.; Aspuru-Guzik, A. Polynomial-time quantum algorithm for the simulation of chemical dynamics. *Proceedings of the National Academy of Sciences* **2008**, *105*, 18681–18686.
- (34) Macridin, A.; Spentzouris, P.; Amundson, J.; Harnik, R. Electron-phonon systems on a universal quantum computer. *Physical review letters* **2018**, *121*, 110504.
- (35) Endo, S.; Sun, J.; Li, Y.; Benjamin, S. C.; Yuan, X. Variational quantum simulation of general processes. *Physical Review Letters* **2020**, *125*, 010501.

- (36) Ollitrault, P. J.; Mazzola, G.; Tavernelli, I. Nonadiabatic molecular quantum dynamics with quantum computers. *Physical Review Letters* **2020**, *125*, 260511.
- (37) Lee, C.-K.; Zhong Lau, J. W.; Shi, L.; Kwek, L. C. Simulating energy transfer in molecular systems with digital quantum computers. *Journal of Chemical Theory and Computation* **2022**, *18*, 1347–1358.
- (38) Tazhigulov, R. N.; Sun, S.-N.; Haghshenas, R.; Zhai, H.; Tan, A. T.; Rubin, N. C.; Babush, R.; Minnich, A. J.; Chan, G. K.-L. Simulating models of challenging correlated molecules and materials on the sycamore quantum processor. *PRX Quantum* **2022**, *3*, 040318.
- (39) Kovyrshin, A.; Skogh, M.; Tornberg, L.; Broo, A.; Mensa, S.; Sahin, E.; Symons, B. C.; Crain, J.; Tavernelli, I. Nonadiabatic nuclear–electron dynamics: a quantum computing approach. *The Journal of Physical Chemistry Letters* **2023**, *14*, 7065–7072.
- (40) Zhang, Y.; Hu, Z.; Wang, Y.; Kais, S. Quantum simulation of the radical pair dynamics of the avian compass. *The Journal of Physical Chemistry Letters* **2023**, *14*, 832–837.
- (41) Gomes, N.; Williams-Young, D. B.; de Jong, W. A. Computing the Many-Body green’s function with adaptive variational quantum dynamics. *Journal of Chemical Theory and Computation* **2023**, *19*, 3313–3323.
- (42) Luo, J.; Lin, K.; Gao, X. Variational quantum simulation of lindblad dynamics via quantum state diffusion. *The Journal of Physical Chemistry Letters* **2024**, *15*, 3516–3522.
- (43) Li, X.; Lyu, S.-X.; Wang, Y.; Xu, R.-X.; Zheng, X.; Yan, Y. Toward quantum simulation of non-Markovian open quantum dynamics: A universal and compact theory. *Physical Review A* **2024**, *110*, 032620.

- (44) Lan, Z.; Liang, W. Integrating Self-Initialized Local Thermalizing Lindblad Operators for Variational Quantum Algorithm with Quantum Jump: Implementation and Performance. *Journal of Chemical Theory and Computation* **2024**, *20*, 10317–10327.
- (45) Lyu, N.; Khazaei, P.; Geva, E.; Batista, V. S. Simulating Cavity-Modified Electron Transfer Dynamics on NISQ Computers. *The Journal of Physical Chemistry Letters* **2024**, *15*, 9535–9542.
- (46) Gallina, F.; Bruschi, M.; Cacciari, R.; Fresch, B. Simulating Non-Markovian Dynamics in Multidimensional Electronic Spectroscopy via Quantum Algorithm. *Journal of Chemical Theory and Computation* **2024**, *20*, 10588–10601.
- (47) Walters, P. L.; Sherazi, M. U.; Wang, F. Variational Quantum Algorithm for Non-Markovian Quantum Dynamics Using an Ensemble of Ehrenfest Trajectories. *The Journal of Physical Chemistry Letters* **2025**, *16*, 1001–1006.
- (48) Dan, X.; Geva, E.; Batista, V. S. Simulating Non-Markovian Quantum Dynamics on NISQ Computers Using the Hierarchical Equations of Motion. *Journal of Chemical Theory and Computation* **2025**, *21*, 1530–1546.
- (49) Chen, M.-C.; Gong, M.; Xu, X.; Yuan, X.; Wang, J.-W.; Wang, C.; Ying, C.; Lin, J.; Xu, Y.; Wu, Y. et al. Demonstration of adiabatic variational quantum computing with a superconducting quantum coprocessor. *Physical Review Letters* **2020**, *125*, 180501.
- (50) Cerezo, M.; Arrasmith, A.; Babbush, R.; Benjamin, S. C.; Endo, S.; Fujii, K.; McClean, J. R.; Mitarai, K.; Yuan, X.; Cincio, L. et al. Variational quantum algorithms. *Nature Reviews Physics* **2021**, *3*, 625–644.
- (51) Tilly, J.; Chen, H.; Cao, S.; Picozzi, D.; Setia, K.; Li, Y.; Grant, E.; Wossnig, L.; Rungger, I.; Booth, G. H. et al. The variational quantum eigensolver: a review of methods and best practices. *Physics Reports* **2022**, *986*, 1–128.

- (52) Peruzzo, A.; McClean, J.; Shadbolt, P.; Yung, M.-H.; Zhou, X.-Q.; Love, P. J.; Aspuru-Guzik, A.; O’Brien, J. L. A variational eigenvalue solver on a photonic quantum processor. *Nature communications* **2014**, *5*, 4213.
- (53) Wecker, D.; Hastings, M. B.; Troyer, M. Progress towards practical quantum variational algorithms. *Physical Review A* **2015**, *92*, 042303.
- (54) Kandala, A.; Mezzacapo, A.; Temme, K.; Takita, M.; Brink, M.; Chow, J. M.; Gambetta, J. M. Hardware-efficient variational quantum eigensolver for small molecules and quantum magnets. *nature* **2017**, *549*, 242–246.
- (55) Lee, J.; Huggins, W. J.; Head-Gordon, M.; Whaley, K. B. Generalized unitary coupled cluster wave functions for quantum computation. *Journal of chemical theory and computation* **2018**, *15*, 311–324.
- (56) Grimsley, H. R.; Economou, S. E.; Barnes, E.; Mayhall, N. J. An adaptive variational algorithm for exact molecular simulations on a quantum computer. *Nature communications* **2019**, *10*, 3007.
- (57) Sim, S.; Johnson, P. D.; Aspuru-Guzik, A. Expressibility and entangling capability of parameterized quantum circuits for hybrid quantum-classical algorithms. *Advanced Quantum Technologies* **2019**, *2*, 1900070.
- (58) Zhang, S.-X.; Wan, Z.-Q.; Lee, C.-K.; Hsieh, C.-Y.; Zhang, S.; Yao, H. Variational quantum-neural hybrid eigensolver. *Physical Review Letters* **2022**, *128*, 120502.
- (59) Fan, Y.; Liu, J.; Li, Z.; Yang, J. Quantum circuit matrix product state ansatz for large-scale simulations of molecules. *Journal of Chemical Theory and Computation* **2023**, *19*, 5407–5417.
- (60) Zeng, X.; Fan, Y.; Liu, J.; Li, Z.; Yang, J. Quantum neural network inspired hard-

- ware adaptable ansatz for efficient quantum simulation of chemical systems. *Journal of Chemical Theory and Computation* **2023**, *19*, 8587–8597.
- (61) Xiao, X.; Zhao, H.; Ren, J.; Fang, W.-H.; Li, Z. Physics-constrained hardware-efficient ansatz on quantum computers that is universal, systematically improvable, and size-consistent. *Journal of Chemical Theory and Computation* **2024**, *20*, 1912–1922.
- (62) Li, W.; Zhang, S.-X.; Sheng, Z.; Gong, C.; Chen, J.; Shuai, Z. Quantum Machine Learning of Molecular Energies with Hybrid Quantum-Neural Wavefunction. *arXiv preprint arXiv:2501.04264* **2025**,
- (63) Fang, J.-Y.; Guo, H. Multiconfiguration time-dependent Hartree studies of the CH₃I/MgO photodissociation dynamics. *The Journal of chemical physics* **1994**, *101*, 5831–5840.
- (64) McLachlan, A. D. A variational solution of the time-dependent Schrodinger equation. *Molecular Physics* **1964**, *8*, 39–44.
- (65) Sawaya, N. P.; Menke, T.; Kyaw, T. H.; Johri, S.; Aspuru-Guzik, A.; Guerreschi, G. G. Resource-efficient digital quantum simulation of d-level systems for photonic, vibrational, and spin-s Hamiltonians. *npj Quantum Information* **2020**, *6*, 49.
- (66) Li, W.; Ren, J.; Huai, S.; Cai, T.; Shuai, Z.; Zhang, S. Efficient quantum simulation of electron-phonon systems by variational basis state encoder. *Physical Review Research* **2023**, *5*, 023046.
- (67) Zhang, S.-X.; Allcock, J.; Wan, Z.-Q.; Liu, S.; Sun, J.; Yu, H.; Yang, X.-H.; Qiu, J.; Ye, Z.; Chen, Y.-Q. et al. Tensorcircuit: a quantum software framework for the nisq era. *Quantum* **2023**, *7*, 912.
- (68) Li, W.; Allcock, J.; Cheng, L.; Zhang, S.-X.; Chen, Y.-Q.; Mailoa, J. P.; Shuai, Z.;

- Zhang, S. TenCirChem: An efficient quantum computational chemistry package for the NISQ era. *Journal of Chemical Theory and Computation* **2023**, *19*, 3966–3981.
- (69) McArdle, S.; Jones, T.; Endo, S.; Li, Y.; Benjamin, S. C.; Yuan, X. Variational ansatz-based quantum simulation of imaginary time evolution. *npj Quantum Information* **2019**, *5*, 75.
- (70) Ollitrault, P. J.; Jandura, S.; Miessen, A.; Burghardt, I.; Martinazzo, R.; Tacchino, F.; Tavernelli, I. Quantum algorithms for grid-based variational time evolution. *Quantum* **2023**, *7*, 1139.
- (71) Yao, Y.-X.; Gomes, N.; Zhang, F.; Wang, C.-Z.; Ho, K.-M.; Iadecola, T.; Orth, P. P. Adaptive variational quantum dynamics simulations. *PRX Quantum* **2021**, *2*, 030307.
- (72) Zhang, Z.-J.; Sun, J.; Yuan, X.; Yung, M.-H. Low-depth Hamiltonian simulation by an adaptive product formula. *Physical Review Letters* **2023**, *130*, 040601.